
Manipulating Single Spins in Quantum Dots Coupled to Ferromagnetic Leads

Matthias Braun¹, Jürgen König¹, and Jan Martinek^{2,3,4}

¹ Institut für Theoretische Physik III, Ruhr-Universität Bochum, 44780 Bochum, Germany

² Institute of Molecular Physics, Polish Academy of Science, 60-179 Poznań, Poland

³ Institut für Theoretische Festkörperphysik, Universität Karlsruhe, 76128 Karlsruhe, Germany

⁴ Institute for Materials Research, Tohoku University, Sendai 980-8577, Japan

We discuss the possibility to generate, manipulate, and probe single spins in single-level quantum dots coupled to ferromagnetic leads. The spin-polarized currents flowing between dot and leads lead to a non-equilibrium spin accumulation, i.e., a finite polarization of the dot spin. Both the magnitude and the direction of the dot's spin polarization depends on the magnetic properties of leads and their coupling to the dot. They can be, furthermore, manipulated by either an externally applied magnetic field or an intrinsically present exchange field that arises due to the tunnel coupling of the strongly-interacting quantum-dot states to spin-polarized leads. The exchange field can be tuned by both the gate and bias voltage, which, therefore, provide convenient handles to manipulate the quantum-dot spin. Since the transmission through the quantum-dot spin valve sensitively depends on the state of the quantum-dot spin, all the dynamics of the latter is reflected in the transport properties of the device.

1 Introduction

The study of single spins in quantum-dot spin valves resides in the intersection of the two highly-interesting and extensively-pursued research fields of spintronics on the one hand and transport through nanostructures on the other hand side. Quantum dots consist of a small confined island with a low capacity such that a macroscopic gate or bias voltage is needed to add a single electron, leading to Coulomb-blockade phenomena [1, 2, 3]. The notion that not only the charge but, simultaneously, also the spin degree of freedom of the electrons can be made use of, for example by using ferromagnetic leads, defines the field of spintronics [4, 5]. A quantum-dot spin valve, i.e., a quantum

dot coupled to ferromagnetic leads, exploits both the spin polarization of the electrons and the sensitivity of the charge to Coulomb interaction. Therefore electronic transport is governed by the behavior of a *single spin*. To discuss the possibility to generate, manipulate, and probe single spins via electronic transport through quantum-dot spin valves is the goal of this chapter.

The capacity C of a metallic or semiconductor island decreases when shrinking its size. For small quantum dots, the energy scale to add a single electron on the island, the charging energy $U = e^2/2C$, exceeds the energy scales set by temperature $k_B T$ or bias voltage eV , and Coulomb-blockade phenomena arise, as first observed by Fulton and Dolan [6]. If, in addition, the island size becomes comparable to the Fermi wavelength then the level spectrum on the island will be discrete. For sufficiently large energy-level spacings, only a single level may participate in transport. Such a system can then be described by the Anderson-impurity model, which is introduced below.

Famous examples of spintronics devices are the spin valves based on either the giant magnetoresistance effect [7] in magnetic multilayers or the tunnel magnetoresistance [8] in magnetic tunnel junctions. These effects arise, when two ferromagnetic leads are in contact via a conducting layer or a tunnel barrier, respectively. The transport characteristics of the device then depend on the relative orientations of the lead magnetizations. If, in a magnetic tunnel junction, the lead magnetizations enclose the angle ϕ , the conductance through the tunnel junction is proportional to $\cos \phi$ [9, 10], i.e., it is maximal for parallel and minimal for antiparallel alignment of the leads' magnetizations. This angular dependence simply reflects the overlap of the spinor part of the majority-spin wave functions in the source and drain electrode, which is given by the externally controlled leads' magnetizations.

This picture changes once spin accumulation can occur. Let us consider transport through a ferromagnet – nonmagnet – ferromagnet sandwich structure with the thickness of the normal layer being smaller than the spin diffusion length. A finite bias voltage applied between the two ferromagnets with nonparallel magnetization directions leads to a local imbalance of spin-up and spin-down electrons in the nonmagnetic layer. This non-equilibrium polarization of the electrons in the nonmagnetic region, known as spin accumulation, mediates the information of the relative orientation of the leads' magnetization through the middle part, such that the transmission through the device is reduced for increasing angle ϕ between directions of the leads' magnetic moments.

An extreme limit of the above scheme is realized in a quantum-dot spin valve. It consists of a quantum dot that is tunnel coupled to ferromagnetic, see Fig. 1. In this case, the information about the relative leads' magnetization directions is mediated by a single quantum-dot electron that, as a consequence of a finite bias voltage is partially spin polarized, described by a finite quantum-statistical average $\mathbf{S} = (\hbar/2)\langle\boldsymbol{\sigma}\rangle$ of the dot spin. It is the orientation of the dot spin relative to the leads together with the degree of the dot spin polarization that determines the transport, rather than just the relative

orientation of the leads' magnetization directions only. Any manipulation of the dot spin polarization will change the transmission through the device.

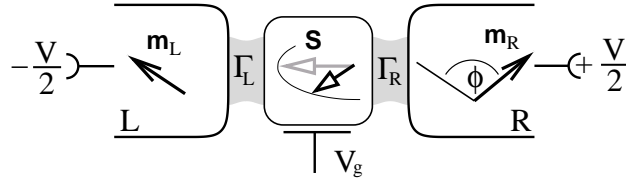


Fig. 1. A quantum dot contacted by ferromagnetic leads with non-collinear magnetizations. The lead magnetization directions enclose the angle ϕ . By forcing a current through the system, a non-equilibrium spin \mathbf{S} accumulates on the otherwise non-magnetic dot.

A quantum-dot spin valve is, thus, a convenient tool to generate, manipulate, and detect spin polarization of single quantum-dot electrons. Both the *generation* and the *detection* of spin polarization on the quantum dot occur via electrical transport as a consequence of spin-polarized charge currents from and to the leads. One of the intriguing features of a quantum-dot spin-valve device is the possibility to further *manipulate* the dot spin. This can be done directly via an externally applied magnetic field [11]. But also the gate and transport voltages influence the dot spin [12, 13, 14, 15]. To understand this, it is important to notice that the strong Coulomb interaction on the quantum dot yields many-body correlations. As for the spin degree of freedom, the quantum-dot electrons are subject to an exchange field that arises as a many-body effect due to the tunnel coupling to spin-polarized leads. This exchange field sensitively depends on the system parameters such as the gate and bias voltage. The latter, therefore, provide suitable handles to manipulate the quantum-dot spin.

Combining ferromagnetic (typically metallic) leads with quantum dots, which are usually semiconductor structures is experimentally challenging. Recent experimental approaches to such a quantum-dot spin valve involve metallic islands [16, 17], granular systems [18], carbon nanotubes [19] as well as single molecules [20] or self-assembled quantum dots [21, 22] coupled to ferromagnetic leads. Another possible realization would rely on contacting a surface impurity acting as quantum dot with a spin-polarized STM tip [23].

Successful demonstration of tunnel magnetoresistance through a strongly interacting system has been reported by Sahoo *et al.* [24] in single-wall carbon nanotubes contacted by PdNi leads, and by Zhang *et al.* in Al grains sandwiched inside a tunnel junction between to Co leads [25].

The article is organized as follows: In Sec. 2 we define the Hamiltonian of the quantum dot coupled to ferromagnetic leads. In Sec. 3 we address the dynamics of the dot spin and charge. Starting from a rigid calculation of the spin and charge current through a tunnel junction, we construct the master/Bloch

equation for the charge/spin degrees of freedom from the charge/spin continuity equation. From the Bloch equation, we discuss, how to prepare, and modify the dot spin via bias voltage, gate voltage and an external applied magnetic field. The so prepared dot spin can be measured by its imprint on the conductance of the quantum dot spin valve device as shown in Sec. 4. We summarize our findings then in Sec. 5.

2 Model Hamiltonian

We describe the quantum-dot spin valve by the following Hamiltonian [12, 13]:

$$H = \sum_{rk\alpha} \varepsilon_{rk\alpha} c_{rk\alpha}^\dagger c_{rk\alpha} + \sum_n \varepsilon_n d_n^\dagger d_n + U d_\uparrow^\dagger d_\uparrow d_\downarrow^\dagger d_\downarrow \quad (1)$$

$$+ \sum_{rk\alpha n} \left(V_{rk\alpha n} c_{rk\alpha}^\dagger d_n + h.c. \right).$$

The first term in Eq. (1) treats the ferromagnetic leads ($r = L/R$) as large reservoirs of itinerant electrons. The Fermion creation and annihilation operators of the lead r are labeled by $c_{rk\alpha}^{(\dagger)}$, where k labels the momentum and $\alpha = \pm$ the spin. The spin-quantization axis for the electrons in reservoir r is chosen along its magnetization direction \mathbf{m}_r . In the spirit of the Stoner model, the property of ferromagnetism is incorporated by assuming an asymmetry in the density of states ξ_α for majority (+) and minority (-) spins. The degree of spin polarization in lead r is characterized by the ratio $p_r = (\xi_{r+} - \xi_{r-}) / (\xi_{r+} + \xi_{r-})$. The lead magnetization directions \mathbf{m}_L and \mathbf{m}_R can enclose an arbitrary angle ϕ . Furthermore, the leads shall be so large, that the electrons can always be described as in equilibrium, i.e. with a Fermi distribution $f_r(\omega)$. An applied bias voltage is taken into account by a symmetric shift of the chemical potential in the left and right lead by $\pm eV/2$.

The quantum dot can be modeled as an Anderson impurity, where d_n^\dagger and d_n are the Fermion creation and annihilation operators of the dot electrons with the spin $n = \uparrow, \downarrow$. The spin quantization axis of the dot is, in general, chosen to be different from the quantization axes of both the left and the right lead. If an external magnetic field is applied, the spin quantization axis is chosen parallel to this field. The energy ε_n of the atomic-like electronic level is measured relative to the equilibrium Fermi energy of the leads, and double occupation of the dot costs the charging energy $U \gg k_B T$.

Electron tunneling between the leads and the dot is described by the last term in Eq. (1). As we have chosen different spin quantization axes for the lead subsystems, parallel to the respective magnetization, the tunneling matrix elements $V_{rk\alpha n}$ are not diagonal in spin space. However, we require that tunneling is spin conserving. The tunneling amplitudes can, then, be separated in $V_{rk\alpha n} = t_{rk} \times U_{\alpha n}^r$, i.e. a spin-independent tunnel amplitude t_{rk} and

a $SU(2)$ rotation matrix $U_{\alpha n}^r$. The explicit shape of the matrix is determined by the choice of the dot spin quantization axis of the dot system.

The tunnel-coupling strength is characterized by the transition rates $\Gamma_{r\alpha}(\omega) = 2\pi \sum_k |t_{rk}|^2 \delta(\omega - \varepsilon_{rk\alpha})$. For simplicity, we assume the density of states ξ_α and the tunneling amplitudes t_r to be independent of energy, which implies constant tunneling rates $\Gamma_{r\alpha}$. The spin asymmetry in the density of states in the leads yields spin-dependent tunneling rates, which are related to the leads' spin polarization by $p_r = (\Gamma_{r+} - \Gamma_{r-})/(\Gamma_{r+} + \Gamma_{r-})$.

Throughout this article we focus on the limit of dot-lead coupling $\Gamma_{r\alpha} \ll k_B T, eV$ when transport is dominated by first-order tunneling, i.e., it is sufficient to calculate all expressions for the charge and spin current up to first order in Γ . This excludes the regimes of second-order transport (cotunneling) in the Coulomb-blockade region [26] or the Kondo regime (see e.g. Ref. [27]).

3 Quantum-Dot-Spin Dynamics

The tunnel coupling of the quantum-dot levels to spin-polarized leads yields a transfer of angular momentum across each of the tunnel junctions. This, together with a change of angular momentum due to an externally applied magnetic field, defines the dynamics of the quantum-dot spin polarization. The stationary value of the latter is determined by balancing all currents of angular momentum. As we discuss in detail below, the total *spin* current, i.e., transfer of angular momentum from the leads to the dot, consists of two qualitatively different contributions. One is associated with the fact that *charge* currents from or to a ferromagnet is spin polarized. This current, thus, transfers angular momentum *along* the magnetization directions of ferromagnet or quantum-dot spin accumulation. There is, however, also an additional contribution of transfer of *perpendicular* angular momentum, which can be expressed in terms of a many-body exchange field acting on the quantum-dot electrons.

For a careful treatment of the total transfer of angular momentum, we first present a rigid calculation of the spin current through a single tunnel junction [28] in terms of non-equilibrium Keldysh Green's functions. This will help us to identify under which circumstances spin currents with perpendicular components will contribute. Afterwards, we specify our result to the weak-coupling regime of a quantum-dot spin valve and derive in this limit Bloch-like rate equations for the quantum-dot spin.

The currents will be functions of the unknown density matrix elements. To derive the stationary density matrix in a non-equilibrium situation, we set the change of charge and spin on the dot equal zero. Then, the Bloch equation for the spin and the continuity equation for the charge degree of freedom from a system of master equations.

3.1 Spin Current Expressed by means of Green's Functions

Our calculation of the spin current in this subsection will be in close analogy to the derivation of the charge current according to Meir and Wingreen [29]. Let us first consider the spin current through one, say the left, tunnel barrier. For a clearer notation, we mostly drop the lead index in this section. The spin current $\mathbf{J}_L = \langle \hat{\mathbf{J}}_L \rangle$ from the lead into the dot is defined by the negative of the time derivative of the total lead spin $\hat{\mathbf{S}}_L = (\hbar/2) \sum_{k\alpha\beta} c_{k\alpha}^\dagger \boldsymbol{\sigma}_{\alpha\beta} c_{k\beta}$, where $\boldsymbol{\sigma}_{\alpha\beta}$ denotes the vector of Pauli matrices. From the Heisenberg equation we get

$$\hat{\mathbf{J}}_L = -\frac{d}{dt} \hat{\mathbf{S}}_L = -\frac{1}{i\hbar} [\hat{\mathbf{S}}_L, H]. \quad (2)$$

Making use of the Fermion commutation relation, we can find the spin-current operator as

$$\hat{\mathbf{J}}_L = -\frac{1}{2i} \sum_{k\alpha\beta n} V_{k\alpha n} \boldsymbol{\sigma}_{\alpha\beta}^* c_{k\beta}^\dagger d_n - V_{k\alpha n}^* \boldsymbol{\sigma}_{\alpha\beta} d_n^\dagger c_{k\beta}. \quad (3)$$

By introducing the Keldysh Green's functions $G_{n,k\beta}^<(t) = i\langle c_{k\beta}^\dagger(0) d_n(t) \rangle$, we can write the expectation value of the spin current as

$$\mathbf{J}_L = \frac{1}{2} \sum_{k\alpha\beta n} \int \frac{d\omega}{2\pi} \left(V_{k\alpha n} \boldsymbol{\sigma}_{\alpha\beta}^* G_{n,k\beta}^<(\omega) - V_{k\alpha n}^* \boldsymbol{\sigma}_{\alpha\beta} G_{k\beta,n}^<(\omega) \right). \quad (4)$$

Since the Green's functions obey the Dyson equations $G_{k\alpha,n}^< = \sum_m V_{k\alpha,m} [g_{k\alpha}^t G_{m,n}^< - g_{k\alpha}^< G_{m,n}^t]$ and $G_{n,k\alpha}^< = \sum_m V_{k\alpha,m}^* [g_{k\alpha}^< G_{n,m}^t - g_{k\alpha}^t G_{n,m}^<]$, we can replace the Green's functions in Eq. (4) with the dot Green's functions $G_{n,m}^<(t) = i\langle d_m^\dagger d_n(t) \rangle$ and the free Green's functions of the lead. The latter are given by $g_{k\alpha}^< = 2\pi i f_L^+(\omega) \delta(\omega - \varepsilon_{k\alpha})$, $g_{k\alpha}^> = -2\pi i f_L^-(\omega) \delta(\omega - \varepsilon_{k\alpha})$, $g_{k\alpha}^{\text{ret}} = 1/(\omega - \varepsilon_{k\alpha} + i0^+)$, and $g_{k\alpha}^{\text{adv}} = (g_{k\alpha}^{\text{ret}})^*$. Here, f_L^+ stands for the Fermi distribution function in the lead L and $f_L^- = 1 - f_L^+$.

If we choose the dot spin quantization axis parallel to the lead magnetization we can substitute the tunnel matrix elements by $V_{k\alpha,n} = t_k \delta_{\alpha n}$. After a lengthy but straightforward calculation, the spin current can be written as

$$\begin{aligned} \mathbf{J}_L = & \frac{i}{4} \sum_{m,n} \int \frac{d\omega}{2\pi} \boldsymbol{\sigma}_{mn} (\Gamma_m + \Gamma_n) [f_L^+(\omega) G_{n,m}^> + f_L^-(\omega) G_{n,m}^<] \\ & + \boldsymbol{\sigma}_{mn} (\Gamma_m - \Gamma_n) \left[f_L^+(\omega) (G_{n,m}^{\text{ret}} + G_{n,m}^{\text{adv}}) + \frac{1}{i\pi} \int' dE \frac{G_{n,m}^<(E)}{E - \omega} \right], \quad (5) \end{aligned}$$

with the tunnel rates $\Gamma_n(\omega) = 2\pi \sum_k |t_{rk}|^2 \delta(\omega - \varepsilon_{rk}) \delta_{\alpha n}$.

This is the most general expression for the spin current flowing through a tunnel barrier. Since the Green's functions $G_{n,m}$ were not specified during the calculation, Eq. (5) holds also for other electronic systems than single-level quantum dots.

If the dot state is rotationally symmetric about \mathbf{m}_L , all dot Green's functions $G_{\sigma\sigma'}$ non-diagonal in spin space vanish. Only in this case, the spin current is proportional to the difference between charge current $I_L^\uparrow = i(e/h) \int d\omega \Gamma_\uparrow [f_L^+(\omega) G_{\uparrow\uparrow}^> + f_L^-(\omega) G_{\uparrow\uparrow}^<]$ carried by spin-up electrons and charge current I_L^\downarrow carried by spin-down electrons,

$$\mathbf{J}_L = J_L^z \mathbf{e}_z = \frac{\hbar}{2e} (I_L^\uparrow - I_L^\downarrow) \mathbf{e}_z \quad (6)$$

If the dot system breaks this rotational symmetry, for example due to spin accumulation along an axis different from \mathbf{m}_L , the simple result of Eq. (6) is no longer correct. In such a situation, the second line in Eq. (5) yields an additional spin-current component, oriented transversal to both, the magnetization of the lead, and the polarization of the dot. This spin-current component describes the exchange coupling between lead and dot spin, causing both to precess around each other. Since the lead magnetization is pinned usually, only the dot spin precesses like in a magnetic field.

Brataas *et al.* [30] showed, that at normal metal – ferromagnet interfaces, incoming electrons, with a spin orientation non-collinear to the magnetization direction, may experience a rotation of the spin direction during backscattering. This mechanism is described by the so called spin-mixing conductance, and also generates a transverse component of the spin current.

3.2 Spin Current Between Ferromagnetic Lead and Quantum Dot

We now specify the above expressions for a quantum-dot spin valve for weak tunnel coupling. Since the expression for the spin current in Eq. (5) does already explicitly depend linearly on the tunnel coupling $\Gamma_{r\sigma}$, we only need the zeroth-order Keldysh Green's functions of the dot system to describe the weak-coupling regime. They are given by

$$G_{\sigma\sigma}^>(\omega) = -2\pi i P_\sigma \delta(\omega - \varepsilon - U) - 2\pi i P_0 \delta(\omega - \varepsilon) \quad (7)$$

$$G_{\sigma\sigma}^<(\omega) = 2\pi i P_\sigma \delta(\omega - \varepsilon) + 2\pi i P_d \delta(\omega - \varepsilon - U) \quad (8)$$

$$G_{\sigma\bar{\sigma}}^>(\omega) = 2\pi i P_\sigma^\sigma \delta(\omega - \varepsilon - U) \quad (9)$$

$$G_{\sigma\bar{\sigma}}^<(\omega) = 2\pi i P_\sigma^\sigma \delta(\omega - \varepsilon) \quad (10)$$

$$G_{\sigma\bar{\sigma}}^{\text{ret}}(\omega) = \frac{P_\sigma^\sigma}{\omega - \varepsilon + i0^+} + \frac{P_\sigma^\sigma}{\omega - \varepsilon + U + i0^+} = (G_{\sigma\bar{\sigma}}^{\text{adv}}(\omega))^* \quad (11)$$

where P_η^χ are the matrix elements of the reduced density matrix of the dot system,

$$\rho_{\text{dot}} = \begin{pmatrix} P_0 & 0 & 0 & 0 \\ 0 & P_\uparrow & P_\uparrow^\dagger & 0 \\ 0 & P_\uparrow^\dagger & P_\downarrow & 0 \\ 0 & 0 & 0 & P_d \end{pmatrix}. \quad (12)$$

The diagonal, real entries $P_\chi \equiv P_\chi^x$ are the probabilities to find the dot in the state empty (0), occupied with a spin up (\uparrow) or down (\downarrow) electron, or double occupied (d) with a spin singlet. The zeros in Eq. (12) in the off diagonals are a consequence of the total-particle-number conservation. The inner 2×2 matrix is the $SU(2)$ representation of the dot spin. The reduced density matrix contains five independent parameters. For convenience, we describe the quantum dot state by the probabilities for the three charge states $P_0, P_1 = P_\uparrow^\uparrow + P_\downarrow^\downarrow$, and P_d (with the normalization condition $P_0 + P_1 + P_d = 1$), and the average-spin vector $\mathbf{S} = (P_\downarrow^\uparrow + P_\uparrow^\downarrow, iP_\downarrow^\uparrow - iP_\uparrow^\downarrow, P_\uparrow^\uparrow - P_\downarrow^\downarrow)/2$.

Similarly to deriving the expression for the spin current, we can get a formula for the charge current I_r through tunnel contact r as

$$I_r = -\frac{e}{h} \sum_{k\alpha n} \int d\omega \left(V_{rk\alpha n} G_{n,rk\alpha}^<(\omega) - V_{rk\alpha n}^* G_{rk\alpha,n}^<(\omega) \right). \quad (13)$$

After choosing a spin-quantization axis for the dot spin and making use of the Dyson equation for the Green's functions, we can plug in the dot Green's function given above to obtain the result

$$I_r = \Gamma_r \frac{2(-e)}{\hbar} \left[f_r^+(\varepsilon) P_0 + \frac{f_r^+(\varepsilon + U) - f_r^-(\varepsilon)}{2} P_1 - f_r^-(\varepsilon + U) P_d - p_r [f_r^-(\varepsilon) + f_r^+(\varepsilon + U)] \mathbf{S} \cdot \mathbf{m}_r \right], \quad (14)$$

that, of course, is independent of the choice of the dot spin's quantization axis. Here, we defined $\Gamma_r \equiv (\Gamma_{r\uparrow} + \Gamma_{r\downarrow})/2$.

It is worth to mention, that the dot spin \mathbf{S} influences the conductance via the scalar product $(\mathbf{S} \cdot \mathbf{m}_r)$. Therefore the tunnel magnetoresistance depends cosine like on the relative angle enclosed by lead magnetization and spin polarization, i.e. it just resembles the behavior of a tunnel junction between two ferromagnetic leads [8, 9, 10].

The first-order spin current, on the other hand, is given by evaluating Eq. (5), which leads to

$$\mathbf{J}_r = \frac{\hbar}{2e} I_r p_r \mathbf{m}_r - \frac{\mathbf{S} - p_r^2 (\mathbf{m}_r \cdot \mathbf{S}) \mathbf{m}_r}{\tau_{c,r}} + \mathbf{S} \times \mathbf{B}_r. \quad (15)$$

The first term describes spin injection from the ferromagnetic lead into the quantum dot by a spin-polarized charge current. The injected spin is proportional to the lead polarization and the electrical current crossing the junction. This spin current contribution vanishes for vanishing bias voltage.

The second term describes relaxation of the dot spin due to coupling to the leads. Since neither an empty nor a doubly-occupied dot can bear a net spin, the spin relaxation time $\tau_{c,r}^{-1} = \Gamma_r/\hbar(1 - f_r(\varepsilon) + f_r(\varepsilon + U))$ equals the life time of the single-occupation dot state. This relaxation term is anisotropic

[31]. The spin polarization of the lead suppresses the relaxation of a dot spin, which is aligned parallel to the lead magnetization.

The third term in Eq. (15) describes transfer of angular momentum perpendicular to the spin-polarization directions of lead and dot. The structure of this terms suggests the interpretation of \mathbf{B}_r as being an effective magnetic field that acts on the quantum-dot spin \mathbf{S} . Its value, in the absence of an external magnetic field, is given by [12, 32]

$$\mathbf{B}_r = p_r \frac{\Gamma_r \hat{\mathbf{n}}_r}{\pi \hbar} \int' d\omega \left(\frac{f_r^+(\omega)}{\omega - \varepsilon - U} + \frac{f_r^-(\omega)}{\omega - \varepsilon} \right), \quad (16)$$

where the prime at the integral indicates Cauchy's principal value. From Eq. (16) it is clear that this field is an exchange field that arises due to the fact that the quantum dot levels are tunnel coupled to a spin-polarized lead. It is a many-body effect as all degrees of freedom in the leads contribute to the integral, and Coulomb interaction in the dot is important not to cancel the first with the second term in the integrand. The exchange field persists also for vanishing bias voltage. A signature of this exchange field in the Kondo-resonance splitting of transport through a single molecule has been observed recently [20], with reported values of the field of up to 70 Tesla.

3.3 Dynamics of the Quantum-Dot Spin

We use the expressions for the charge and spin current, Eqs. (14) and (15), to calculate the dynamics of the dot's charge and spin. Strictly speaking, above calculation holds only for static systems. To emphasize the physical origin of the following equations, we keep all time derivatives in this section, even if they should have the numerical value of zero.

The continuity equation of the average dot charge $\langle n \rangle = \sum_n n P_n$ is given by

$$e \frac{d\langle n \rangle}{dt} = I_L + I_R. \quad (17)$$

Moreover, not only the total charge current through the dot is conserved, but also the charge current through the individual charge levels. Therefore we can split the charge continuity Eq. 17 into the two contributions associated with transport processes in which either double occupied or an empty dot is involved. The affiliation to either contribution is indicated by the arguments of the Fermi functions, where the presence of the interaction energy U indicates processes with double occupation and the absence signals processes involving an empty dot. We get

$$\begin{aligned} \frac{dP_0}{dt} &= \sum_r \Gamma_r \left(f_r^+(\varepsilon) P_0 - f_r^-(\varepsilon) P_1/2 - p_r f_r^-(\varepsilon) \mathbf{S} \cdot \mathbf{m}_r \right) \\ \frac{dP_d}{dt} &= \sum_r \Gamma_r \left(f_r^+(\varepsilon + U) P_1/2 - f_r^-(\varepsilon + U) P_d - p_r f_r^+(\varepsilon + U) \mathbf{S} \cdot \mathbf{m}_r \right). \end{aligned} \quad (18)$$

Similar to the charge continuity equation, the continuity equation for the dot spin reads

$$\begin{aligned} \frac{d\mathbf{S}}{dt} &= \mathbf{J}_L + \mathbf{J}_R + \mathbf{S} \times \mathbf{B}_{\text{ext}} - \frac{\mathbf{S}}{\tau_{\text{rel}}} \\ &= \frac{\hbar}{2e} \sum_r \left[I_r p_r \mathbf{m}_r - \frac{\mathbf{S} - p^2(\mathbf{m}_r \cdot \mathbf{S})\mathbf{m}_r}{\tau_{c,r}} \right] + \mathbf{S} \times \mathbf{B}_{\text{tot}} - \frac{\mathbf{S}}{\tau_{\text{rel}}}. \end{aligned} \quad (19)$$

with $\mathbf{B}_{\text{tot}} = (\mathbf{B}_L + \mathbf{B}_R + \mathbf{B}_{\text{ext}})$. In addition to the spin currents entering the quantum dot from the left and right lead, there is one term describing spin precession due to an external magnetic field \mathbf{B}_{ext} . It enters the equation in the same way as the exchange field with the left and right reservoir, so that all three of them add up to the total field \mathbf{B}_{tot} . Furthermore, we phenomenologically took into account the possibility of intrinsic spin relaxation, e.g., due to spin-orbit coupling, hyperfine interaction with nuclei in the quantum dot, or higher-order tunnel processes such as spin-flip cotunneling, with a time scale τ_{rel} . The total spin-decoherence time of the dot spin is, therefore, given by

$$(\tau_s)^{-1} = (\tau_{\text{rel}})^{-1} + (\tau_{c,L})^{-1} + (\tau_{c,R})^{-1}. \quad (20)$$

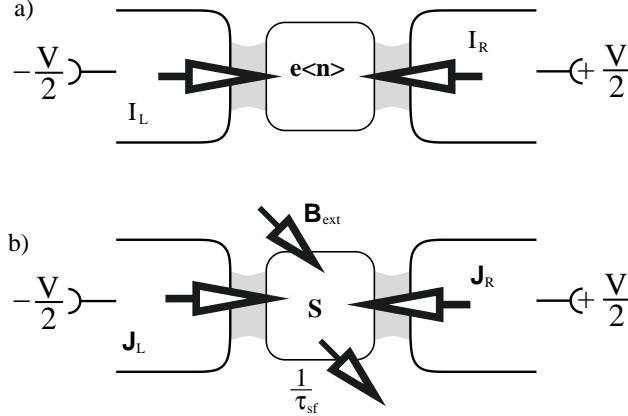


Fig. 2. a) The dot charge changes according to the electrical current through the tunnel barriers. b) The dot spin changes according to the spin currents through the tunnel barriers. In addition, an external magnetic field acts as additional source and the intrinsic spin relaxation as sink of angular momentum.

The different handles to manipulate the quantum-dot spin are comprised the total field \mathbf{B}_{tot} . It contains the external magnetic field \mathbf{B}_{ext} as a direct tool to initiate a spin precession. However, also the the exchange fields can be used for this task [13]. As we see from Eq. (16), the exchange field depends on both the gate and bias voltage via the level position ε and the Fermi distribution functions $f_r(\omega)$.

4 Manipulation and Detection of the Quantum-Dot Spin via Electrical Transport

Since the spin state of the quantum dot enters the expressions for the charge current in Eq. (14), any manipulation on the quantum-dot spin can be detected in measuring the dc -charge current through the device.

In order to calculate the charge current, we need to determine the stationary solution for the density matrix, i.e. for the dot spin \mathbf{S} and the charge occupation probabilities P_i . For these six variables, we need six independent equations: the probability normalization condition $\sum_n P_n = 1$, the Bloch equation $d\mathbf{S}/dt = 0$ (contains three equations), and the two equations originating from the charge continuity.

In the following we analyze stationary transport situations, i.e., neither the charge nor the spin of the dot changes with time, and the currents through the left and right tunnel junction are equal $I_L = -I_R \equiv I$. For simplicity, we choose symmetric coupling $\Gamma_L = \Gamma_R = \Gamma/2$, equal spin polarizations $p_L = p_R = p$, and a symmetrically applied bias $V_R = -V_L = V/2$ for the following discussion.

In the following three subsection we consider the effect of the gate and transport voltage as well as an external magnetic field on the quantum-dot spin, and how this is reflected by electric transport through the quantum-dot spin valve. Then, in reversal, by experimentally measuring the transport characteristics of the device, one can conclude the spin state of the quantum dot.

4.1 Gate Voltage Effect in Linear Response Regime

To study the effect of the gate voltage on the quantum-dot spin via the gate-voltage dependence of the exchange field, we analyze the linear-response regime in the absence of an external magnetic field, and for simplicity without intrinsic spin relaxation. Without any applied bias voltage $V = 0$, i.e. in equilibrium the stationary solution of the rate equations for the charge occupation probabilities (18) is given by the Boltzmann distribution, $P_\chi \sim \exp(-E_\chi/k_B T)$, and no current flows. Since the dot itself is non-magnetic, the dot spin vanishes $\mathbf{S} = 0$. For a small bias voltage $eV \ll k_B T$, we can expand the master Eq. (19) and (18) up to linear order in V . With symmetric couplings to the left and right lead, the charge probabilities (P_0, P_1, P_d) become independent on V , thus, the occupation probabilities are given by their equilibrium value, but the spin degree of freedom is not. The linear charge current, which is polarized due to the lead magnetizations generate a finite dot-spin polarization along $p(\mathbf{m}_L - \mathbf{m}_R)$, i.e., along the y axis in the coordinate system defined in Fig. 3.

The damping term in Eq. (19) limits the magnitude of spin accumulation. The term $\mathbf{S} \times (\mathbf{B}_L + \mathbf{B}_R)$ yields an intrinsic precession of the spin around the

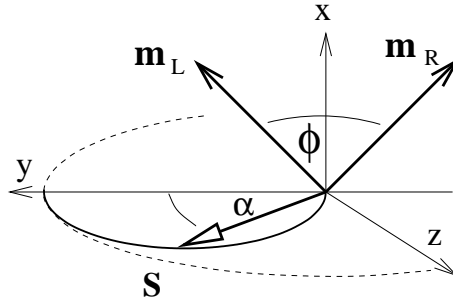


Fig. 3. Spin dynamics in the linear-response regime. Spin accumulates along the y direction. The spin precesses due to the exchange field that is along the x direction. Therefore, the stationary solution of the average spin on the dot is tilted away from the y axis by an angle α , plotted in Fig. 4(b).

exchange field $\mathbf{B}_L + \mathbf{B}_R \equiv B_0 \cos(\phi/2) \mathbf{e}_x$. In the steady state, the average dot spin is rotated by the angle

$$\alpha = -\arctan\left(B_0 \tau_s \cos \frac{\phi}{2}\right). \quad (21)$$

Therefore the accumulated spin acquires both y and z components as seen in Fig. 3. This precession also reduces the magnitude of the accumulated spin to

$$|\mathbf{S}| = p I \tau_s \cos \alpha. \quad (22)$$

The precession angle α is plotted in Fig. 4(b) as function of the level position ε , that can be tuned by the gate voltage. The angle α changes its sign at $\varepsilon = -U/2$, due to a sign change of the exchange field at this point. The level position $\varepsilon = -U/2$ is special, since then the particle and hole like processes generating the exchange field compensate each other.

As pointed out above, in the linear-response regime under consideration the charge occupation probabilities do not depend on the spin polarization of the leads. In particular, they are independent of the relative angle ϕ of the leads' magnetization. This means that the ϕ dependence of the conductance is determined by the product $\mathbf{S} \cdot \mathbf{m}_L = -\mathbf{S} \cdot \mathbf{m}_R$, as can be seen from Eqs. (14). It is the relative orientation of the accumulated spin and the drain (or source) that produces the ϕ dependence of the current, rather than the product $\mathbf{m}_L \cdot \mathbf{m}_R$, as in the case of a single magnetic tunnel junction. Therefore the ϕ dependent linear conductance $G^{\text{lin}} = (\partial I / \partial V)|_{V=0}$ directly reflects the accumulated spin. The effect of the exchange field for the normalized conductance is seen from the analytic expression

$$\frac{G^{\text{lin}}(\phi)}{G^{\text{lin}}(0)} = 1 - p^2 \frac{\sin^2(\phi/2)}{1 + (B_0 \tau_s)^2 \cos^2(\phi/2)}, \quad (23)$$

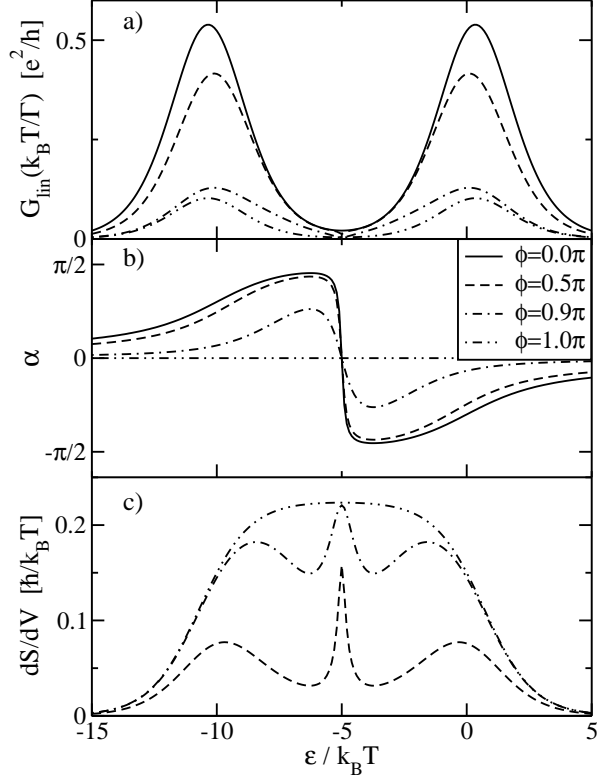


Fig. 4. (a) Linear conductance normalized by $\Gamma/k_B T$ as a function of the level position ε for different angles ϕ . (b) Angle α enclosed by the accumulated spin and the y axis as defined in Fig. 3. (c) Derivation of the magnitude of the accumulated spin on the dot with respect to the source-drain voltage V . Further parameters are $p = 0.9$ and $U = 10k_B T$.

which is plotted in Fig. 5 for different values of the level position ε .

For $\varepsilon > 0$, the quantum dot is predominantly empty, and for $\varepsilon + U < 0$ doubly occupied with a spin singlet. In this regions, the life time of a singly-occupied dot τ_c is short, and so is the lifetime of the dot spin. Therefore the rotation angle α is small and the normalized conductance as a function of the relative angle ϕ of the lead magnetizations shows a harmonic behavior, see, e.g., the curve for $\varepsilon = 5k_B T$ in Fig. 5.

For $-U < \varepsilon < 0$ the dot is primarily singly occupied, so the spin dwell time is increased and the exchange field becomes important. It causes the above described spin precession, which decreases the product $\mathbf{S} \cdot \mathbf{m}_L$ since the relative angle between \mathbf{m}_L and \mathbf{S} is increased and the magnitude of \mathbf{S} is reduced. Thus, the spin precession makes the spin-valve effect less pronounced, leading to a

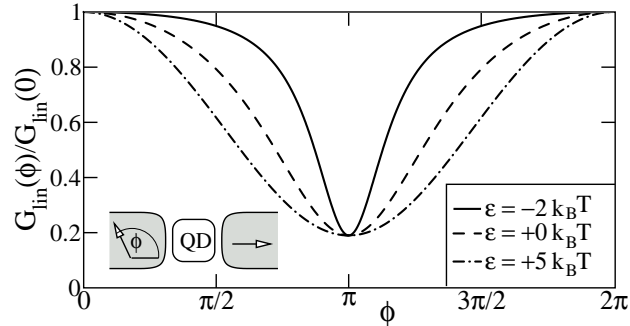


Fig. 5. Normalized conductance as a function of the angle ϕ enclosed by the lead magnetization for different level positions and the parameters $U = 10k_B T$ and $p = 0.9$.

value of the conductance that exceeds the expectations made by Slonczewski in Re. [9] for a single magnetic tunnel junction.

For parallel and antiparallel aligned lead magnetizations, $\phi = 0$ and $\phi = \pi$, the accumulated spin and the exchange field also get aligned. In this case, the spin precession stops, even though the exchange field is still present. The ϕ -dependent conductance is not affected by the exchange field at this alignment, see Fig. 5.

4.2 Bias Voltage Effect in Non-Linear Regime

We now turn to the non-linear response regime, $eV > k_B T$, in order to discuss the effect of the bias-voltage dependence of the exchange field on the quantum-dot spin. Again, we assume that there is no external magnetic field, and no spin relaxation.

In Fig. 6(a) we show the current I as a function of the bias voltage V for an antiparallel configuration of the leads' magnetizations and different values of the leads' spin polarization p .

For non-magnetic leads, the current-voltage characteristic shows the usual Coulomb staircase. At low bias voltage, the dot is empty and transport is blocked. With increasing bias voltage, first single and then double occupancy of the dot is possible, which opens first one and then two transport channels. A finite spin polarization p leads to spin accumulation and, thus, to a reduction of transport. A reduction of transport with increasing p is also seen for noncollinear magnetization. But there is a qualitative difference as can be seen in Fig. 6(b). A very pronounced negative differential conductance evolves out of the middle plateau as p is increased. To understand the negative differential conductance we first neglect the exchange field and then, in a second step, analyze how the exchange field modifies the picture.

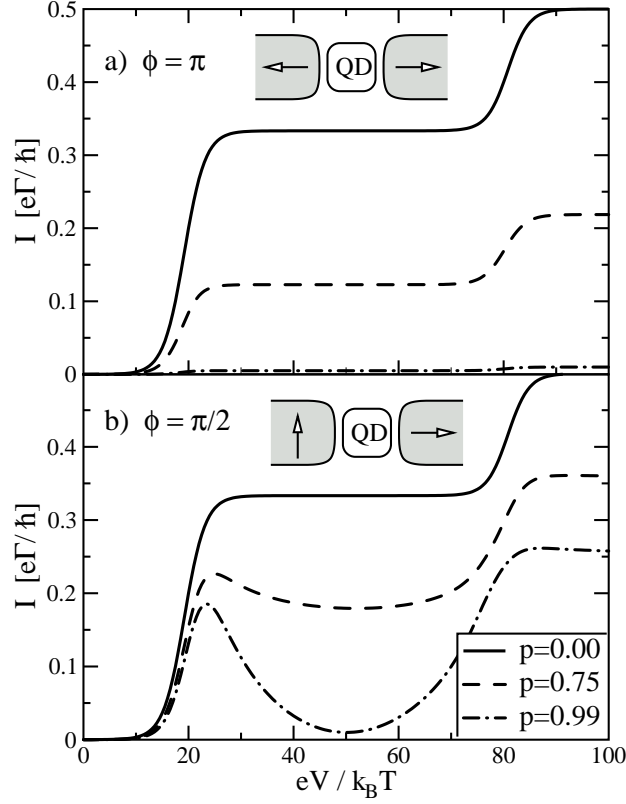


Fig. 6. Current-voltage characteristics for antiparallel (a) and perpendicular aligned (b) lead magnetizations. Further parameters are $\Gamma_L = \Gamma_R = \Gamma/2$, $p_L = p_R = p$, $\varepsilon = 10k_B T$, and $U = 30k_B T$.

At the intermediate bias voltages, the dot can only be empty or singly occupied, double occupation is forbidden. Therefore all electrons entering the dot through the left barrier find an empty dot. In this regime the current $I = (e\Gamma/\hbar)P_0$ explicitly depends only on the probability to find the dot empty. The transport through the dot must be suppressed by charge accumulation on the dot, i.e., $P_1 \rightarrow 1$ and $P_0 \rightarrow 0$.

The origin of this charge accumulation becomes clear from the relation of charge and spin

$$\mathbf{S} = p \left[\frac{\Gamma_L}{\Gamma_R} P_0 \mathbf{m}_L - \frac{1 - P_0}{2} \mathbf{m}_R \right]. \quad (24)$$

If, in the steady state, the dot is primarily occupied by one electron, this electron has a spin, which is antiparallel aligned to the drain lead. Due to this

antiparallel alignment, the tunneling rate to the drain lead is maximally suppressed, while the tunnel coupling to the source lead is not as much affected. When the rate to the drain lead is weak, but strong to the source lead, then the dot is primarily occupied by one electron.

The transport is suppressed, since an electron is trapped due to its spin alignment, and no second electron can enter the dot because of the Coulomb interaction. So this mechanism is a type of spin blockade but with a different physical origin compared to the systems described in literature [33, 34]. The suppression defines the local minimum of the current in Fig. 6(b). At this point, the relevant exchange field component generated by the coupling to the left lead vanishes, so that spin precession becomes insignificant. Away from this point spin precession sets in as illustrated in Fig. 7. The spin rotates about \mathbf{m}_L , the spin blockade gets lifted, and the electron can now more easily leave the dot via the drain electrode.

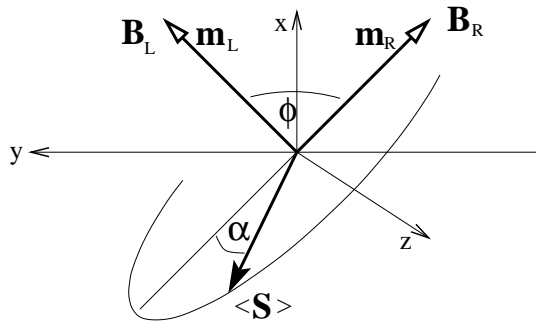


Fig. 7. For electrons polarized antiparallel to the drain lead, the influence of the effective field generated by the source lead is dominating. By rotating the spins, the spin blockade is lifted and therefore the conductance recovers.

The particular value of the non-linear conductance is a consequence of the two competing effects. Spin blockade reduces, while spin precession again increases the conductance. Since the strength of the exchange field varies as a function of the level position with respect to the Fermi level, see Fig. 8(a), this recovery is non-monotonous, what leads to a negative differential conductance. To illustrate this further, we plot in Fig. 8(b) the current which we obtained when the spin precession contribution is in an artificial way dropped in Eq. (19), and compare it with the total current. In the absence of the exchange field, a wide plateau is recovered, whose height is similar to the current, one would expect, if the lead magnetizations were aligned antiparallel. The peak at the left end of the plateau indicates that, once the dot level is close to the Fermi level of the source electrode, the spin blockade is relaxed since the dot electrons have the possibility to leave to the left side.

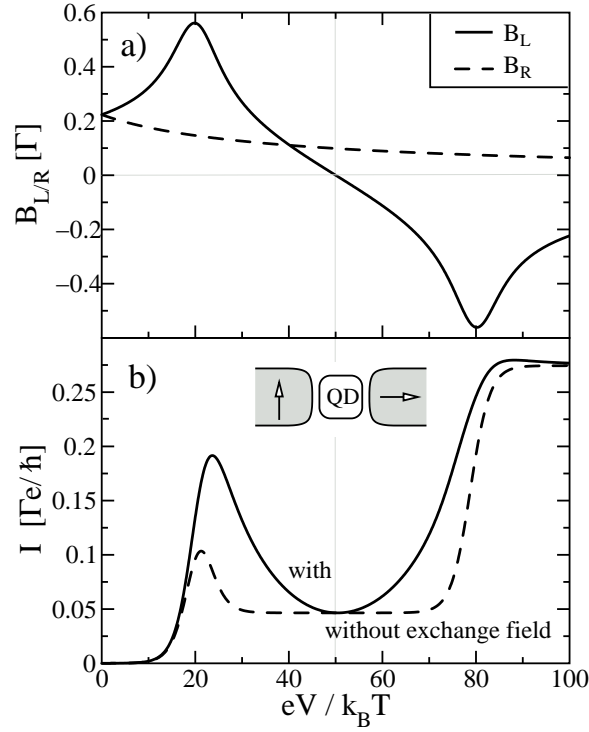


Fig. 8. Panel (a) The absolute value of the effective exchange field contributions from the left and right leads. Panel (b) the current voltage dependence, with and without the influence of the exchange field. For both plots the parameters $\phi = \pi/2$, $\Gamma_L = \Gamma_R = \Gamma/2$, $\varepsilon = 10k_B T$, $U = 30k_B T$, and $p = 0.95$ were chosen.

However, this negative differential conductance occur only at relatively high values of the lead polarization. For symmetric tunnel coupling a spin polarization of $p \approx 0.77$ is needed, while for a strong asymmetry in the tunnel coupling the required spin polarization is reduced.

The effect of the spin blockade on the ϕ -dependent of the current is depicted in Fig. 9. We choose the bias voltage according to $eV/2 = \varepsilon + U/2$, such that the influence of the exchange field is absent. For $p = 0.5$ still a $\sin^2 \frac{\phi}{2}$ dependence can be recognized. For higher values of the spin polarization the conductance drops faster and stays nearly constant at its minimal value due to spin blockade. This is just the opposite behavior than predicted for the linear-response regime as seen in Fig. 5.

If such a high bias voltage is applied, that the dot can also be double occupied, the step-like behavior of the current voltage characteristic is recov-

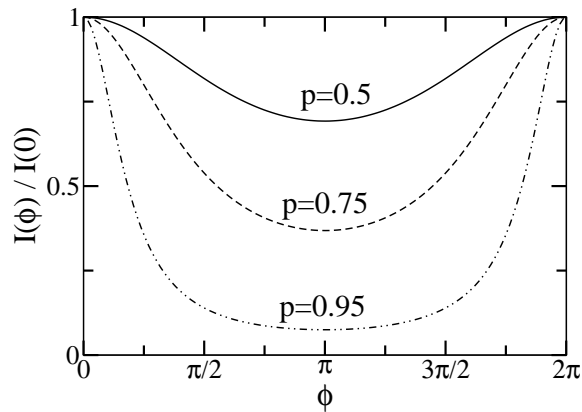


Fig. 9. Angular dependence of the conductance with an applied voltage of $V = \varepsilon + U/2$, i.e., the voltage generating the smallest influence of the exchange field. Further plot parameters are $\Gamma_L = \Gamma_R = \Gamma/2$, $p_L = p_R = p$, $\varepsilon = 10k_B T$, and $U = 30k_B T$.

ered, see Fig. 6(b). Away from the step, all appearing Fermi functions can be approximated by 0 or 1, and following Eq. (14) the current is given by $I = (e\Gamma/2\hbar)[1 - p\mathbf{S} \cdot (\mathbf{m}_L - \mathbf{m}_R)]$. Far away from the resonance, where the exchange field can be neglected, the accumulated spin is $\mathbf{S} = p(\mathbf{m}_L - \mathbf{m}_R)/4$ from which we get

$$I = \frac{e\Gamma}{2\hbar} \left(1 - p^2 \sin^2 \frac{\phi}{2} \right). \quad (25)$$

The suppression of transport due to the spin polarization p of the leads is comparable with the case of a single-tunnel junctions, when charging effects are of no importance.

We close this section with the remark that while we plotted only results for the case $\varepsilon > 0$, in the opposite case $\varepsilon < 0$ the current-voltage characteristics is qualitatively the same.

4.3 External Magnetic Field

In the previous subsections were studied quantum-dot spin dynamics that is evoked by the exchange field. But one also make use of an externally-applied magnetic field \mathbf{B}_{ext} . It turns out that with an external field one can measure the spin-decoherence time T_2 . To emphasize this point, we explicitly allow intrinsic spin relaxation on the dot. Then, we observe a separation of the charge life time $\tau_c^{-1} = \tau_{c,L}^{-1} + \tau_{c,R}^{-1}$ and the spin life time on the dot $\tau_s^{-1} = \tau_c^{-1} + \tau_{\text{rel}}^{-1}$

An external field leads to the Hanle effect [11], *i.e.*, the decrease of spin accumulation in the quantum dot due to precession about a static magnetic field. Indeed, this was the effect used by Johnson and Silsbee [35] and others [17] to prove non-equilibrium spin accumulation.

Optical realizations of such Hanle experiments [36] always involve an ensemble averaging over different dot realizations, so the outcome of the measurement is T_2^* rather than T_2 . By measuring the Hanle signal via the conductance through a quantum dot attached to ferromagnetic leads, this ensemble averaging is avoided.

In a recent experiment Zhang *et. al.* [25] realized this kind of setup but with a whole layer of aluminum dots in a tunnel junction between two Co electrodes. Even so the measurements involve averaging over different realizations of the dots, multi levels and local magnetizations, they clearly observe a Hanle resonance in the magnetoresistance of the device.

For simplicity we assume symmetric couplings $\Gamma_L = \Gamma_R$, equal degree of lead polarizations $p_L = p_R = p$ and consider the linear-response regime only. There is a variety of possible relative orientations of the external field and the leads' magnetizations to each other. In the following, we consider two specific cases in detail, as they are convenient to extract useful information about the spin-decoherence time in one case, and to prove the existence of the exchange field in the other one.

Antiparallel Aligned Lead' Magnetizations

We first focus on two ferromagnetic leads with magnetization directions antiparallel to each other, see Fig. 10, and an arbitrary aligned external field. The configuration has the advantage that the exchange field contributions from the two leads cancel, and the spin dynamics is only govern by the external field \mathbf{B}_{ext} . The linear conductance, then, is

$$\frac{G}{G_0} = 1 - p^2 \frac{\tau_s}{\tau_c} \frac{1 + (\frac{m_L - m_R}{2} \mathbf{B}_{\text{ext}} \tau_s)^2}{1 + (\mathbf{B}_{\text{ext}} \tau_s)^2}. \quad (26)$$

where $G_0 = e^2 P_1 / \tau_c k_B T$ is the asymptotic value of the conductance for a large magnetic field, $|\mathbf{B}_{\text{ext}}| \rightarrow \infty$, for which the spin accumulation is completely destroyed. The latter is proportional to the single occupation probability P_1 .

If we assume the field to be aligned perpendicular to the lead magnetizations (see Fig. 10), we find the Lorentzian dependence on the external magnetic field that is familiar from the optical Hanle effect. The depth of the dip is given by $p^2 \tau_s / \tau_c$ while the width of the dip in Fig. 10 provides a direct access to the spin lifetime τ_s . Of course, the conversion of applied magnetic field to frequency requires the knowledge of the Lande factor g , which must be determined separately like in Ref. [22].

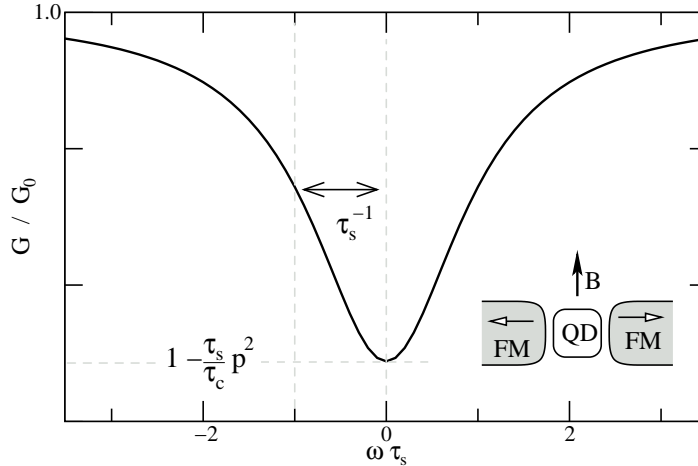


Fig. 10. Differential conductance, for ferromagnetic leads with anti-parallel magnetization, as a function of the magnetic field ω applied perpendicular to the accumulated spin. The half line width of the Hanle resonance directly determines the spin-decoherence time τ_s .

Magnetic Field Applied Along $\mathbf{m}_L + \mathbf{m}_R$

Finally, we discuss the case of a non-collinear configuration of the leads' magnetizations with a magnetic field applied along the direction $\mathbf{m}_L + \mathbf{m}_R$ as shown in Fig. 11.

In this case, both the exchange field and the external magnetic field are pointing along the same direction $\mathbf{m}_L + \mathbf{m}_R$, so their magnitude is just added. The linear conductance is, then,

$$\frac{G}{G_0} = 1 - p^2 \frac{\tau_s}{\tau_c} \frac{\sin^2 \frac{\phi}{2}}{1 + (\mathbf{B}_{\text{ext}} + \mathbf{B}_L + \mathbf{B}_R)^2 \tau_s^2}, \quad (27)$$

where ϕ is the angle enclosed by \mathbf{m}_L and \mathbf{m}_R . The conductance as function of applied magnetic field as plotted in Fig. 11(a) reaches its minimal value when the sum of external and exchange field vanishes. The exchange field leads to a shift of the minimum's position relative to $|\mathbf{B}_{\text{ext}}| = 0$ [13]. In real experiments, depending on the particular sample geometry, one can expect a magnetic stray field, which is not considered to be part of the experimentally applied magnetic field \mathbf{B}_{ext} . These stray fields also lead to a shift of the conductance minimum. However, the analyzed setup of external field and magnetizations' directions allows for a stringent experimental verification of spin precession due to the exchange field. To separate the exchange field from the influence of possible stray fields its gate voltage dependence can be used. The exchange interaction as function of the dot gate voltage is plotted in the inset of Fig. 11(b). While the stray fields does not depend on gate voltage, the exchange field does. In

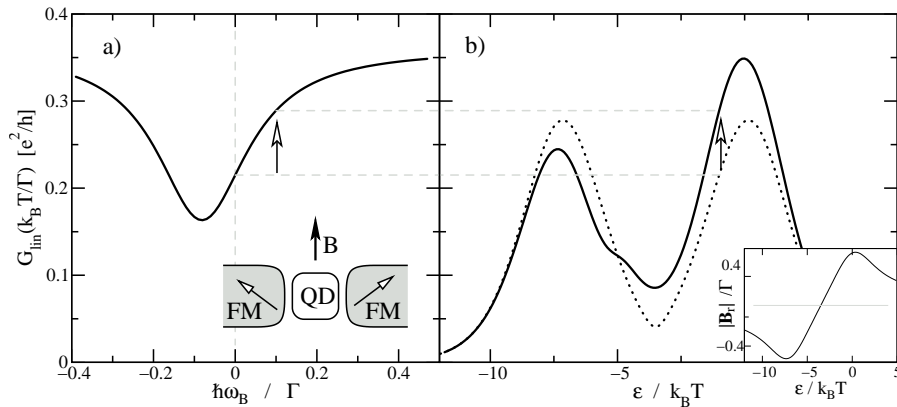


Fig. 11. Linear conductance of the dot for an applied external magnetic field \mathbf{B}_{ext} along $\mathbf{m}_L + \mathbf{m}_R$. a) Linear conductance as a function of the applied field for $\varepsilon = 0$. b) Linear conductance as a function of the level position ε without external field (dotted) and for the applied field $|\mathbf{B}_{\text{ext}}| = 0.1\Gamma/\hbar$ (solid). Further parameters are $\phi = 3\pi/4$, $p = 0.8$, $U = 7k_B T$, and $\tau_{\text{rel}} = 0$. The vertical lines relate the conductance increase of the dot at $\varepsilon = 0$ for a magnetic field $\hbar\omega_B = 0.1\Gamma$.

the flat band limit it even changes sign as a function of gate voltage. By plotting the conductance as function of the gate voltage in Fig. 11(b), we can observe the typical Coulomb blockade oscillations, when the energy level of the empty or singly-occupied dot becomes resonant with the lead Fermi energy. The interplay of exchange and external field leads to an increase of conductance for one resonance peak, but to a decrease for the other resonance.

5 Conclusions

We discussed the possibility to generate, manipulate, and probe single spins in single-level quantum dots coupled to ferromagnetic leads. A finite spin-polarization of the quantum-dot electron is achieved by spin-polarized charge currents from or to the leads at finite bias voltage. Any manipulation of the accumulated spin, e.g. by an external magnetic field or by an intrinsic exchange field, is detectable in the electric current through the device. The occurrence of the exchange field is a consequence of many-body correlations that are one of the intriguing features of nanostructures with large Coulomb interaction.

We determine the dynamics of the quantum-dot spin by deriving expressions for the spin currents through the tunnel barriers. In addition to a contribution that is associated with the spin-polarization of the charge currents from or to ferromagnets, there is a second contribution describing transfer of angular momentum perpendicular to the leads' and dot's magnetization that can be expressed in terms of the exchange field.

In order to manipulate the quantum-dot spin we suggest to make use of the gate- and bias voltage dependence of the exchange field or to apply an external magnetic field. In particular, the spin precession modifies the dependence of the linear conductance on the opening angle of the lead magnetizations. The degree of modification is tunable by the gate voltage. In nonlinear response, the bias-voltage dependence of the exchange field can give rise to a negative differential conductance. An application of a tunable external magnetic field allows one to determine the dot-spin lifetime and to verify the existence of the intrinsic spin precession caused by the exchange coupling.

Acknowledgments

We thank J. Barnaś, G. Bauer, A. Brataas, P. Brower, D. Davidovic, B. Kubala, S. Maekawa, D. Ralph, G. Schön, D. Urban, and B. Wunsch for discussions. This work was supported by the DFG under CFN, SFB 491, and GRK 726, the EC RTN on 'Spintronics', Project PBZ/KBN/044/P03/2001 and the EC Contract G5MACT-2002-04049.

References

1. D.V. Averin, K.K. Likharev: in *Mesoscopic Phenomenon in Solids*, ed. by B.L. Altshuler, P.A. Lee, R.A. Webb (Amsterdam: North-Holland 1991)
2. *Single Charge Tunneling: Coulomb Blockade Phenomena in Nanostructures*, NATO ASI Series B: Physics 294, ed. by H. Grabert, M.H. Devoret (Plenum Press, New York 1992)
3. *Mesoscopic Electron Transport*, ed. by L.L. Sohn, L.P. Kouwenhoven, G. Schön (Kluwer, Dordrecht 1997)
4. S. A. Wolf, D. D. Awschalom, R. A. Buhrman, J. M. Daughton, S. von Molnár, M. L. Roukes, A. Y. Chtchelkanova, D. M. Treger, *Science*, **294**, 1488-1495 (2001)
5. I. Zutic, J. Fabian, and S. Das Sarma, *Rev. Mod. Phys.* **76**, 323 (2004)
6. T. A. Fulton and G. J. Dolan, *Phys. Rev. Lett.* **59**, 109 (1987)
7. M. N. Baibich, J. M. Broto, A. Fert, F. Nguyen Van Dau, F. Petroff, P. Etienne, G. Creuzet, A. Friederich, and J. Chazelas, *Phys. Rev. Lett.* **61**, 2472 (1988).
8. M. Jullière, *Phys. Lett. A* **54**, 225 (1975).
9. J. C. Slonczewski, *Phys. Rev. B* **39**, 6995 (1989).
10. J. S. Moodera and L. R. Kinder, *J. Appl. Phys.* **79**, 4724 (1996); H. Jaffrès, D. Lacour, F. Nguyen Van Dau, J. Briatico, F. Petroff, and A. Vaurès, *Phys. Rev. B* **64**, 064427 (2001).
11. M. Braun, J. König, and J. Martinek, *Europhys. Lett.* **72**, 294 (2005).
12. J. König and J. Martinek, *Phys. Rev. Lett.* **90**, 166602 (2003).
13. M. Braun, J. König, and J. Martinek, *Phys. Rev. B* **70**, 195345 (2004).
14. S. Braig and P. W. Brouwer, *Phys. Rev. B* **71**, 195324 (2005).
15. G. Usaj and H. U. Baranger, *Phys. Rev. B* **63**, 184418 (2001); G. Usaj and H. U. Baranger, *Phys. Rev. B* **71**, 179903 (E) (2005).

16. K. Ono, H. Shimada, and Y. Ootuka, *J. Phys. Soc. Jpn.* **66**, 1261 (1997).
17. M. Zaffalon and B. J. van Wees, *Phys. Rev. Lett.* **91**, 186601 (2003).
18. L. F. Schelp, A. Fert, F. Fettar, P. Holody, S. F. Lee, J. L. Maurice, F. Petroff, and A. Vaurés, *Phys. Rev. B* **56**, R5747 (1997); K. Yakushiji, S. Mitani, K. Takanashi, S. Takahashi, S. Maekawa, H. Imamura, and H. Fujimori *Appl. Phys. Lett.* **78**, 515 (2001).
19. A. Jensen, J. Nygård and J. Borggreen in *Proceedings of the International Symposium on Mesoscopic Superconductivity and Spintronics*, edited by H. Takayanagi and J. Nitta, (World Scientific 2003), pp. 33-37; B. Zhao, I. Mönch, H. Vinzelberg, T. Mühl, and C. M. Schneider, *Appl. Phys. Lett.* **80**, 3144 (2002); K. Tsukagoshi, B. W. Alphenaar, and H. Ago, *Nature* **401**, 572 (1999).
20. A. N. Pasupathy, R. C. Bialczak, J. Martinek, J. E. Grose, L. A. K. Donev, P. L. McEuen, and D. C. Ralph, *Science*, **306**, 86 (2004).
21. Y. Chye, M. E. White, E. Johnston-Halperin, B. D. Gerardot, D. D. Awschalom, and P. M. Petroff, *Phys. Rev. B* **66**, 201301(R) (2002).
22. M. M. Deshmukh and D. C. Ralph, *Phys. Rev. Lett.* **89**, 266803 (2002).
23. A. Kubetzka, M. Bode, O. Pietzsch, and R. Wiesendanger, *Phys. Rev. Lett.* **88**, 057201 (2002).
24. S. Sahoo, C. Schönenberger et al., *Nature Physics* **1**, 102 (2005).
25. L. Y. Zhang, C. Y. Wang, Y. G. Wei, X. Y. Liu, and D. Davidović, *Phys. Rev. B* **72**, 155445 (2005).
26. I. Weymann, J. Barnas, J. König, J. Martinek, and G. Schön, *Phys. Rev. B* **72**, 113301 (2005); I. Weymann, J. König, J. Martinek, J. Barnas, and G. Schön, *Phys. Rev. B* **72**, 115334 (2005).
27. J. Martinek, Y. Utsumi, H. Imamura, J. Barnas, S. Maekawa, J. König, and G. Schön, *Phys. Rev. Lett.* **91**, 127203 (2003); J. Martinek, M. Sindel, L. Borda, J. Barnas, J. König, G. Schön, and J. von Delft, *Phys. Rev. Lett.* **91**, 247202 (2003).
28. M. Braun, J. König, and J. Martinek, *Superlat. and Microstruc.* **37**, 333 (2005).
29. Y. Meir and N. S. Wingreen, *Phys. Rev. Lett.* **68**, 2512 (1992).
30. A. Brataas, Y. V. Nazarov, and G. E. W. Bauer, *Eur. Phys. J B* **22**, 99 (2001).
31. A. Brataas, Y. Tserkovnyak, G. E. W. Bauer, and B. I. Halperin, *Phys. Rev. B* **66**, 060404(R) (2002).
32. J. König, J. Martinek, J. Barnas, and G. Schön, in "CFN Lectures on Functional Nanostructures", Eds. K. Busch *et al.*, *Lecture Notes in Physics* **658**, Springer, 145-164 (2005).
33. D. Weinmann, W. Häusler, and B. Kramer, *Phys. Rev. Lett.* **74**, 984 (1995); A. K. Huettel, H. Qin, A. W. Holleitner, R. H. Blick, K. Neumaier, D. Weinmann, K. Eberl, and J. P. Kotthaus, *Europhys. Lett.* **62**, 712 (2003).
34. K. Ono, D. G. Austing, Y. Tokura, and S. Tarucha, *Science* **297**, 1313 (2002).
35. M. Johnson and R. H. Silsbee, *Phys. Rev. Lett.* **55**, 1790 (1985); *Phys. Rev. B* **37**, 5326 (1988).
36. R. J. Epstein, D. T. Fuchs, W. V. Schoenfeld, P. M. Petroff, and D. D. Awschalom, *Appl. Phys. Lett.* **78**, 733 (2001).

